Enhanced methanol production over non-promoted Cu-MgO-Al_2O_3 materials with ex-solved 2 nm Cu particles: Insights from an Operando spectroscopic study

Jorge Cored[a], Jaime Mazarío[a], Cristina Cerdá-Moreno[a], Pablo G. Lustemberg[b,c], M. Verónica Ganduglia-Pirovano[b], Marcelo E. Domine[a], Patricia Concepción[a,*]

[a] *Instituto de Tecnología Química, Universitat Politècnica de València-Consejo Superior de Investigaciones Científicas (UPV-CSIC), Avenida de los Naranjos s/n, 46022 Valencia, Spain*

[b] *Instituto de Catálisis y Petroleoquímica, CSIC, C/Marie Curie 2, 28049 Madrid, Spain*

[c] *Instituto de Fisica Rosario (IFIR), CONICET-UNR, Bv. 27 de Febrero 210bis, 2000EZP Rosario, Santa Fe, Argentina*

- **ABSTRACT**

Enhanced methanol production is obtained over a non-promoted Cu-MgO-Al_2O_3 mixed oxide catalyst derived from a Cu-Mg-Al hydrotalcite precursor (HT) containing narrowly distributed small Cu NPs (2 nm). Conversions close to the equilibrium (~20%) with a methanol selectivity of 67% are achieved at 230 °C, 20 bar and space velocity of 571 $mL \cdot g_{cat}^{-1} \cdot h^{-1}$. Based on operando spectroscopic studies, the striking activity of this Cu based catalyst is ascribed to the stabilization of Cu^+ ions favored under reaction conditions due to lattice reorganization associated with the "HT-memory effect", promoted by water. Temperature resolved IR-MS experiments have enabled the discernment of monodentate formate species, stabilized on Cu^+ as the intermediate in methanol synthesis, in line with the results of DFT calculations. These monodentate formate species are much more reactive than bridge formate species, behaving the last ones as intermediates in methane and CO formation. Moreover, poisoning of the Cu^0 surface by strongly adsorbed species behaving as spectators is observed under reaction conditions. This work represents a detailed spectroscopic study highlighting the influence of the reaction pressure on the stabilization of active surface sites, and the possibility of enhancing methanol production on usually less active non-promoted nano-sized copper catalysts, providing that the proper support is selected, allowing the stabilization of doped Cu^+. Thus, methanol formation rate of $2.6 \cdot 10^{-3} mol_{MeOH} \cdot g_{cat}^{-1} \cdot h^{-1}$ at 230 °C, 20 bar and WHSV = 28500 $mL \cdot g_{cat}^{-1} \cdot h^{-1}$, is obtained on the Cu-MgO-Al_2O_3 HT-derived catalyst with 71% methanol selectivity, compared to $2.2 \cdot 10^{-4}$ $mol_{MeOH} \cdot g_{cat}^{-1} \cdot h^{-1}$ with 54% methanol selectivity obtained on a reference Cu/(Al_2O_3-MgO) catalyst not derived from a HT structure.

Keywords CO_2, methanol, copper, IR spectroscopy, operando spectroscopy, hydrotalcite.

▪ INTRODUCTION

Establishing a carbon-neutral economy is one of the main targets in our society. In this context, greenhouse gas recycling, where the CO_2 released into the atmosphere is captured and converted into chemicals and fuels, represents a hotspot in catalysis research as a means to close the carbon cycle.[1-4] Accordingly, the methanol synthesis from CO/CO_2 hydrogenation is attracting widespread interest since CO_2 is a critical platform chemical with a total annual production of 95 million tonnes per year in 2019.[5,6] On this point, high catalyst efficiency is one of the most pursued challenges researchers are dealing with. One appealing way to enhance the catalytic performance in many processes is to decrease the size of the active component to the nano- or sub-nanometer range, thus increasing the number of exposed surface atoms and the density of low-coordinated surface sites. This results in most cases in greater activity for smaller particle sizes.[7] However, an opposite trend has been reported in the methanol synthesis from CO/CO_2 hydrogenation, where the activity decreases significantly for Cu particles smaller than 8 nm,[8] specifically when using inert or non-redox supports in the absence of promoters.[9,10] Additionally, it has been reported that, with decreasing particle sizes, CO formation by the reverse water gas shift reaction (RWGS) starts to dominate versus methanol synthesis,[11] resulting in a low catalytic efficiency. In this sense, the possibility to develop new synthetic strategies, whereby it might be possible to modify the selectivity and inactivity of small particle size catalysts, is of particular significance from an economic efficiency viewpoint. This becomes especially interesting when using non redox supports, low metal loadings (<10%) and in the absence of promoters. In this respect, Yu et al. reported the possibility of enhancing methanol production by stabilizing Cu^+ ions in a shattuckite-like structure in a 17 wt% Cu/SiO_2 catalysts containing highly dispersed 2.6-3.8 nm copper particles prepared by flame spray pyrolysis.[12] Methanol yield of ~$1.1\cdot10^{-3}$ mol $_{MeOH}\cdot g_{cat}^{-1}\cdot h^{-1}$ at 230 °C and 30 bar (CO_2:H_2 molar ratio 1 to 3; GHSV = 2040 h^{-1}) is obtained, surpassing that of conventional Cu/SiO_2 catalysts, which have been usually considered as inert catalysts.[9-11] In other studies, Cu/Al_2O_3 catalysts containing other metal oxides like MgO, CaO, SrO and BaO with a Cu:Me:Al molar ratio of 50:30:20 and prepared by a co-precipitation method have been investigated. Methanol yields of $5.1\cdot10^{-4}$ $mol_{MeOH}\cdot g_{cat}^{-1}\cdot h^{-1}$ and 31% selectivity to methanol at 200 °C and 20 bar (CO_2:H_2 molar ratio 1 to 2.8; GHSV = 2000 h^{-1}) have been reported for the most active $Cu/MgO/Al_2O_3$ catalyst.[13] In analogy, low methanol selectivity (29.8% at 4.3% CO_2 conversion) has been reported for copper catalysts supported on MgO-modified by TiO_2[14] and for Cu-doped $MgAl_2O_4$ catalysts containing nano-sized Cu NP (1-5 nm) displaying methanol selectivity below 20% at 2% CO_2 conversion.[15] In summary, all these results converge in an insufficient activity when non-promoted catalysts using non-redox supports are considered.

Aiming at enhancing the activity of small Cu NPs, Copéret et al., using a surface organometallic chemistry method, obtained well and narrowly distributed Cu NPs (2-4 nm) on a SiO_2 support decorated with different types of promoters acting as Lewis acid sites, i.e., Ti^{4+}, Zr^{4+}, Ga^{3+} and Zn^{2+}.[16-19] Without a promoter, the catalyst shows poor activity, being enhanced after adding the second metal. In this case, methanol formation rates up to $1.7 \cdot 10^{-4}$ $mol_{MeOH} \cdot g_{cat}^{-1} \cdot h^{-1}$ with 86% methanol selectivity is obtained at 230 °C, 25 bar (CO_2:H_2 molar ratio 1 to 3 and WHSV = 24000 $mL \cdot g_{cat}^{-1} \cdot h^{-1}$) on a Cu-$Zn^{II}$@$SiO_2$ catalyst, composed of 4 nm Cu NPs, and 4.16 wt% Cu and 1.62 wt% Zn.[19]

As a precursor of well dispersed metal species, layered double hydroxides (LDH) with hydrotalcite-like structure and a general formula $[M^{2+}_{1-x}M^{3+}_{x}(OH)_2]^{z+} \cdot [A^{n-}_{z/n} \cdot mH_2O]^{z-}$ have shown great interest in catalysis. Although most of the material comprises low-cost earth available elements (Mg-Al), the possibility to introduce a wide range of chemical compositions and structural features make them suitable catalysts in many organic transformations.[20] In particular, due to their basicity, they proved to be excellent candidates for CO_2 capture and utilization.[21,22] In this regard, many catalyst's formulations, including divalent (Ni^{2+}, Co^{2+}, Mg^{2+}, Cu^{2+}, Zn^{2+}) and trivalent cations (Fe^{3+}, Ga^{3+}, Al^{3+}, Mn^{3+}, …) have been reported, resulting in complex bi- and multi-metallic systems with interesting CO_2 hydrogenation activity to methanol.[21-24] In the simplest formulation, containing only one metal besides Mg^{2+} and Al^{3+}, most studies have been focused on Ni^{2+} and Co^{2+},[21] and recently on Cu^{2+} giving in those cases CO and CH_4.[25] In particular, in the latter case, a reduced Cu-Mg-Al LDH derived catalyst, with basicity and operating conditions selected explicitly for the RWGS reaction displayed an enhanced specific activity towards CO due to the improved CO_2 adsorption on the material.

Consequently, seeking cost-efficient and non-promoted copper based catalysts with high atom efficiency in the synthesis of methanol from CO_2 hydrogenation, hydrotalcite-derived materials seem to be a promising alternative. Therefore, and supported on our previous experience in hydrotalcite-like materials,[26] a Cu-MgO-Al_2O_3 mixed oxide catalyst containing small Cu NPs (2 nm) and moderate basicity, derived from a Mg-Al-Cu hydrotalcite (HT) precursor has been explored in this work. Despite the absence of promoters and the redox inertness of the support, this catalyst appears as an interesting candidate in the CO_2 hydrogenation to methanol with high thermal and temporal stability.

Thus, methanol formation rate of $2.6 \cdot 10^{-3}$ $mol_{MeOH} \cdot g_{cat}^{-1} \cdot h^{-1}$ at 230 °C, 20 bar, CO_2:H_2 molar ratio 1 to 3 and WHSV = 28500 $mL \cdot g_{cat}^{-1} \cdot h^{-1}$, has been obtained with 71% methanol selectivity outperforming that of analogous non-promoted nano-sized Cu-based catalysts. The beneficial role of the HT-derived structure in the catalytic performance of the aforementioned catalyst has been highlighted compared to a Cu/Al_2O_3/MgO reference catalyst not derived from a HT

structure. In particular, catalyst restructuration under reaction conditions, promoted by the so-called water-induced "HT-memory effect" and the positive effect of Cu^+ ions in enhancing methanol formation have been compellingly disentangled by using operando IR-MS spectroscopic studies combined with IR surface titration experiments. In that way, monodentate formate species have been determined as a crucial intermediate in Cu^+ promoted methanol synthesis, shining a light on the ambiguity of literature studies. DFT calculations on model undoped and Cu-doped MgO surfaces have contributed to the assignment of the nature of formate species.

▪ EXPERIMENTAL SECTION

Synthesis of CuHT-230 and CuHT-450. Hydrotalcite-type materials were prepared by a co-precipitation through a mesoscale flow synthesis procedure described elsewhere.[27-29] Besides, and to maximize the yield and bring forth a material with satisfactory physicochemical properties, synthesis and aging conditions (i.e., pH, temperature, time) were selected according to a recent optimization described in ref 26. The synthesis method started from two different aqueous solutions. On the one hand, solution A, containing the metallic species (i.e., Mg, Al, Cu) in the desired molar ratios to achieve a M^{II}/M^{III} mol ratio ~4 as nitrates (i.e., $Mg(NO_3)_2{\cdot}6H_2O$, $Al(NO_3)_3{\cdot}9H_2O$ and $Cu(NO_3)_2{\cdot}2.5H_2O$, from Sigma-Aldrich) and 1.5 M of total cationic concentration. On the other hand, solution B, with the same total mass as solution A, but containing sodium carbonate (Fisher) and sodium hydroxide (Scharlab) in adequate amounts to accomplish a CO_3^{2-} / (sol. A total cationic number) molar ratio equal to 0.66 and OH^- / (sol. A overall positive charge) molar ratio equal to 1, respectively. These solutions were added at the same rate (20 $mL{\cdot}h^{-1}$) to an empty beaker with continuous stirring at 200 rpm and room temperature. After that, precipitates were aged at 60 °C overnight under sealed conditions, without agitation. The resulting solids were filtered, washed with Milli-Q water until pH ~7, and dried overnight at 100 °C. Finally, the hydrotalcite was calcined at 550 °C for 6 h under static air to attain the corresponding mixed oxide. Before their use in catalysis and for spectroscopic measurements, the mixed oxides were in-situ reduced under an H_2 flow (20 $mL{\cdot}min^{-1}$) at either 230 °C (CuHT-230) or 450 °C (CuHT-450), always using a ramp rate = 5 $°C{\cdot}min^{-1}$ and for 3 h at maximum temperature.

Synthesis of Cu/HT (w) and Cu/HT (ACN). Initially, the pure hydrotalcite material used as support (HT; just containing Mg and Al as metallic species) was synthesized following the same procedure above described for the Cu-Mg-Al hydrotalcite-derived materials. Nonetheless, in this case, the hydrotalcite was calcined at 450 °C (2 $°C{\cdot}min^{-1}$, for a total time of 10 h) under an airflow (100 $mL{\cdot}min^{-1}$) to attain the corresponding Mg-Al mixed oxide, as usually performed for simple

Mg-Al hydrotalcites.[27,30] The incorporation of copper onto this support was carried out by the incipient wetness impregnation method using a solution of $Cu(NO_3)_2 \cdot 2.5H_2O$ in water (w) or in acetonitrile (ACN) at an adequate concentration to achieve a metal loading of ~10 wt% in the final solid. The latter solvent (i.e., ACN) was used alternatively to avoid the presence of water during the impregnation process, minimizing the HT memory effect. The impregnated solid was dried in a stove at 100 °C for 24 h (Cu/HT (w)) or in a fume hood at room temperature for 6h (Cu/HT (ACN)). Afterwards, the catalytic system was calcined at 550 °C (3 °C·min^{-1}, 5 h) under air. Finally, the catalyst was thermally reduced at 230 °C (5 °C·min^{-1}) under a H_2 flow (20 mL·min^{-1}) for 3 h, prior to their use in catalytic experiments.

Synthesis of Cu/(Al_2O_3/MgO). An intimate physical mixture of Al_2O_3 and MgO was used to support Cu nanoparticles for comparative purposes. This composite was prepared by incorporating $Al(NO_3)_3 \cdot 9H_2O$ onto a high surface area MgO (MgO Nanoactive Plus, Nanoscale Corp.) by incipient wetness impregnation, followed by a calcination program analogous to that used for the pure Mg-Al hydrotalcites. The amount of $Al(NO_3)_3 \cdot 9H_2O$ was calculated to keep the M^{II}/M^{III} at the same value used throughout this work (i.e., ~4), aiming at achieving acid-base properties analogous to those obtained for the HT-derived materials. Afterwards, copper was incorporated onto this support by incipient wetness impregnation using an aqueous solution of $Cu(NO_3)_2 \cdot 2.5H_2O$, at an adequate concentration to achieve a metal loading of ~10 wt% in the final solid. Finally, the catalyst was thermally reduced at 230 °C (5 °C·min^{-1}) under a H_2 flow (20 mL·min^{-1}) for 3 h, prior to their use in catalytic experiments.

Synthesis of Cu/SiO_2. Nonporous silica spheres were synthesized *via* a technique adapted from Stöber et al.[31] Then, copper was deposited *via* incipient wetness impregnation, followed by drying and calcination. Before impregnation, the SiO_2 support was dried at 150 °C under vacuum for 1 h to remove adsorbed water. After that, the support was impregnated with an aqueous solution (0.1M HNO_3) of copper nitrate ($Cu(NO_3)_2 \cdot 3H_2O$, Sigma-Aldrich) with the adequate concentration to achieve 1.5 wt% of Cu in the final material. The material was dried overnight under vacuum, at room temperature. Subsequently, the sample (~1 g) was heated at 350 °C (2 °C·min^{-1}) in a flow reactor with 750 mL·min^{-1} of N_2.

Copper content, and hydrotalcite and mixed oxide compositions were characterized by Inductively Coupled Plasma Optical Emission Spectrometry (ICP-OES), with a Varian 715-ES ICP-Optical Emission spectrometer, after sample digestion in an HNO_3/HCl aqueous solution for those materials containing Mg, and HNO_3/HCl/HF aqueous solution for the Cu/SiO_2 sample.

X-ray diffraction (XRD) measurements were performed using a PANalytical Cubix Pro diffractometer with a CuK_α X-ray source (λ=0.15406 nm), provided with a variable divergence

slit and working in fixed irradiated area mode. Data were collected over a 2θ range of 5–90° at a scan rate of 2 min^{-1}, operating at 40 kV and 35 mA. Spectra were compared with the PDF2 database (codes in parenthesis) for adequate identification.

Surface areas of solid samples (250 mg) were calculated by applying the Brunauer–Emmett–Teller (BET) model to the range of the N_2 adsorption isotherm where a linear relationship is maintained. These isotherms were obtained from liquid nitrogen adsorption experiments at −196 °C, in a Micromeritics flowsorb apparatus.

High-resolution transmission electron microscopy (HR-TEM) images were collected on a 200 kV Jeol JEM-2100F instrument. The microscope was also equipped with a high-angle annular dark-field (HAADF) detector to be run in a STEM mode, thereby achieving better compositional contrast between Cu-NPs and the oxide support. In this manner, the particle size distribution for each reduced samples was obtained with its statistical parameters (the $\pm$ σ value). In all cases, a minimum number of 200 particles was considered. This study was done employing an image analyser software (ImageJ). The instrument also had an EDX X-Max 80 detector, with a resolution of 127 eV, which supplied qualitative information about which elements were in the sample. Therefore, maps with different colours depending on the element were obtained. These analyses allowed us to confirm the presence of copper nanoparticles as the bright dots in the STEM images. Additionally, Field Emission Scanning Electron Microscopy images were collected on a Zeiss Gemini SEM 500 instrument for the sample Cu/SiO_2 to check that the Stöber silica support was prepared correctly.

Temperature-programmed reduction (TPR-H_2) analysis were performed on a Micromeritics Autochem 2910 instrument. About 50 mg of sample were initially cleaned with 30 $mL{\cdot}min^{-1}$ of Ar at room temperature for 30 min. Then a mixture of 10 vol % of H_2 in Ar was passed through the solid at a total flow rate of 50 $mL{\cdot}min^{-1}$, while the temperature was increased up to 800 °C at a heating rate of 10 $°C{\cdot}min^{-1}$. The H_2 consumption was measured using a thermal conductivity detector (TCD), previously calibrated using the reduction of CuO as a reference.

The amount of **surface copper metal sites** was measured by N_2O surface oxidation[32,33] followed by TPR-H_2 analysis in a Micromeritics Autochem 2910 instrument assuming an adsorption stoichiometry of 1:2 (H_2:Cu). Before measurements, about 50 mg of catalyst was activated in 20 $mL{\cdot}min^{-1}$ H_2 flow (3 h, 230 °C for CuHT-230 sample). After reduction, the sample was cleaned at the same temperature under Ar flow. Then, the temperature was decreased to 25 °C and the surface is oxidised using N_2O (1 vol % in He, 10 $mL{\cdot}min^{-1}$, 1h) from Cu^0 to Cu_2O. After this, the sample was cleaned with Ar (15 min) at room temperature. Finally, a TPR-H_2 was carried on until 400 °C (10 vol % H_2 in Ar, 50 $mL{\cdot}min^{-1}$, 10 $°C{\cdot}min^{-1}$) in order to reduce the previous oxidized Cu_2O to Cu^0.

The copper surface area has been calculated as: $Cu_{surf,area}$ (m^2_{Cu}/g_{cat}) = ($\frac{mol_{Cu,surf}}{g_{cat}} \cdot N_A / C_M$), and the mass of exposed copper has been calculated as: $Mass_{Cu,surf}$ (g_{Cu}/g_{cat}) = ($\frac{mol_{Cu,surf}}{g_{cat}} \cdot 63.546$ g/mol), where $\frac{mol_{Cu,surf}}{g_{cat}}$ is determined from the amount of H_2 consumed to reduce the surface of copper particles ($Cu_2O \rightarrow Cu^0$) that have been previously oxidized by N_2O, applying a factor considering the 1:2 (H_2:Cu) stoichiometry; N_A is the Avogadro's number; C_M is the number of surface Cu atoms per unit surface area ($1.47 \cdot 10^{19}$ at/m^2); 63.546 g/mol is atomic weight of copper.

Temperature Programmed Desorption (TPD-CO_2) studies over *in situ* reduced samples were performed using a quartz reactor, connected online to a mass spectrometer Balzer (QMG 220M1). 100 mg of sample was first activated in a 20 mL·min^{-1} H_2 flow at 230 °C (5 °C·min^{-1}) for 3 h. Then, the sample was flushed with Ar (18 mL·min^{-1}) and the temperature decreased to RT. After stabilization, CO_2 was pulsed 19 times using a four way-valve (100 µL loop). After the adsorption, the temperature was increased to 600 °C, maintaining the inert flow (10 °C·min^{-1}). CO_2 desorption was followed by MS (*m/z*=44).

Infrared (IR) spectra were recorded with a Nicolet (Nexus) 8700 FTIR spectrometer using a DTGS detector and acquiring at 4 cm^{-1} resolution. For IR measurements, samples were pressed into self-supported wafers and submitted to activation conditions prior to each experiment.

IR characterization of reduced materials using CO as probe molecule was carried out by treating the samples at 230 °C (or 450 °C for CuHT-450 sample) in H_2 flow (10 mL·min^{-1}, 2.5 h), followed by evacuation at 10^{-4} mbar at 150 °C for 1.5 h and cooling down to -170 °C under dynamic vacuum conditions. CO was dosed at -170 °C and at increasing pressure (up to 5 mbar). IR spectra were recorded after each dosage. Spectra deconvolution has been done using the Origin software. In a first instance, derived curves and the parameters involved in the Gaussian fitting (i.e., y_0, x_c, w, and A) associated to the support were obtained. With these values, the IR spectra of the copper containing samples were deconvoluted.

Operando CO_2 hydrogenation IR studies at atmospheric pressure were performed in a home-made IR catalytic cell connected "online" to a mass spectrometer (Balzer (QMG 220 M1)). The IR cell allows *in situ* treatments in controlled atmospheres and temperatures from -176 °C to 500 °C, connected to a vacuum system with a gas dosing facility. Samples were firstly reduced in H_2 flow (see above). After activation, the temperature was decreased to 160 °C, and the gas feed switched to reaction conditions (20 mL·min^{-1} total flow, 5 mL·min^{-1} CO_2, and 15 mL·min^{-1} H_2). After 15 min of stabilization and monitored by MS, the temperature was increased to 200 °C and kept there for 30 min. After this reaction step, the temperature was set at 230 °C for

another 30 min. IR spectra were acquired after all the experimental steps and every 15 min during catalysis. After the reaction, the temperature was decreased to 180 °C, followed by evacuation at 10^{-1} mbar (primary pump Leybold). Once the sample is at RT, the system is cooled down to -170 °C under dynamic vacuum conditions (10^{-4} mbar, using TBM pump, Pfeiffer). CO was dosed at -170 °C and at increasing pressure (up to 5 mbar). IR spectra were recorded after each dosage.

Operando CO_2 hydrogenation IR studies at 9 bar pressure were performed in a commercial IR catalytic cell (Aabspec, model #2000-A, *https://www.aabspec.com/newproducts.html)* connected "online" to a mass spectrometer (Balzer (QMG 220 M1)). This type of experiment initially presents the same two first steps that the CO_2 hydrogenation at atmospheric pressure (activation + reaction at 1 bar, see the previous procedure above). After 1 bar reaction, the temperature was decreased to 160 °C, removing CO_2 from the gas mixture and fixing 25 mL·min^{-1} pure H_2. Then, a back pressure regulator (BPR, Swagelok), connected in the outlet port of the IR-cell, was constrained to increase the pressure to 9 bar. After pressurization, the reaction mixture (20 mL·min^{-1} total flow, 5 mL·min^{-1} CO_2 and 15 mL·min^{-1} H_2) was submitted into the cell and stabilized for 15-30 min. Then, the temperature was increased to 230 °C and kept there for 2 h. IR spectra were acquired after all the experimental steps and every 15 min during catalysis. The reaction was monitored by online MS as well as by offline GC. A three-way valve was installed before the MS instrument, to extract the downstream gas through a plastic syringe to the latter tracking. After 2 h on stream, the temperature was decreased to 180 °C and the cell was depressurized. The cell evacuation and the CO titration experiment were performed by following the previous subsection procedure at a temperature of -170 °C.

Hydrogenation experiments after operando IR CO_2+H_2 reaction were performed at 1 and 9 bar. The experimental procedure until the hydrogenation step has already been explained above for both pressures. After reaction, the temperature was decreased to 100 °C and the gas mixture switched to 30 mL·min^{-1}; 10 vol% H_2/N_2. Then, a progressive hydrogenation at increasing temperatures and H_2 % vol concentration was carried out. Further details can be found in **SI**.

Mass analysis was performed using a mass spectrometer Balzer (QMG 220 M1) coupled to IR reaction cells. The m/z values used to monitor each compound were: 44 (CO_2), 31 (MeOH), 29 (HCOH), 28 (CO), 18 (H_2O), 15 (CH_4) and 2 (H_2). Additionally, m/z values of 3 (HD), 4 (D_2), 34 (CH_2DOD), 19 (CHD_3) and 20 (CD_4) were monitored during IR isotopic experiments (see **SI**).

Laboratory XPS spectra of the catalysts were recorded with a SPECS spectrometer equipped with a Phoibos 150 MCD-9 multichannel analyzer using a non-monochromatic AlK_α (1486.6 eV) X-Ray source. Spectra were recorded with an X-Ray power of 50 W, pass energy of 30 eV, and under an operating pressure of 10^{-9} mbar. The sample (~30-50 mg) was pressed into a pellet

and loaded onto a SPECS stainless steel sample holder. Before XPS analysis, the samples were submitted to different treatments in a high-pressure reactor (HPCR) connected under UHV to the XPS analysis chamber: i) H_2 reduction (10 mL·min^{-1} flow) at 230 °C and atmospheric pressure for 3 h; ii) CO_2 hydrogenation reaction at 230 °C and 1 and 9 bar pressures in a CO_2:H_2 mixture (1:3 molar ratio, 8 mL·min^{-1} total flow) for 2 h. Gases were flown through two mass flow controllers (Bronkhorst). XPS spectra were referenced to the Mg 1s peak (1303.86 eV) and Si 2p peak (103.5 eV). Data treatment was addressed using the CASA XPS software.

CO_2 hydrogenation catalytic test were performed in a stainless-steel fixed bed reactor (inner diameter of 11 mm and 240 mm length), equipped with a back pressure regulator (BPR, Swagelok) that allows working at a pressure range of 1-20 bar. Typically, 200 mg of catalyst (particle size 400-600 μm) was diluted in SiC in a weight ratio 0.13 (Cat/SiC). Samples were *in situ* reduced at atmospheric pressure prior to catalytic tests (20 mL·min^{-1} H_2, 230 °C, 3 h, 5 °C·min^{-1} for all samples; 450 °C for CuHT-450 sample). Experiments at a constant weight hourly space velocity (WHSV, ~28500 mL·g_{cat}^{-1}·h^{-1}) were performed under concentrated reaction conditions (23.8 vol % CO_2, 71.3 vol % H_2, 5 vol % N_2) at 20 bar and reaction temperatures from 230 to 280 °C. Each temperature was maintained for at least 1.5 h. Catalytic experiments were also performed at different contact times (WHSV ~570 to 134000 mL·g_{cat}^{-1}·h^{-1}), maintaining the 3:1 H_2 to CO_2 molar ratio at 20 bar pressure. The thermal stability of the CuHT-230 sample was evaluated at 230 °C after 3 high temperature steps at 280 °C (45, 90 and 90 min) and 20 bar (WHSV, 5700 mL·g_{cat}^{-1}·h^{-1}). In addition, a long-term stability experiment was carried out at 230 °C and 20 bar (WHSV, 5700 mL·g_{cat}^{-1}·h^{-1}) for 85 h. Direct analysis of the reaction products was done by online gas chromatography (GC), using a SCION-456-GC equipment with TCD (MS-13X column) and FID (BR-Q Plot column) detectors. Blank experiments (in the presence of SiC) showed the absence of a homogeneous contribution to the reaction.

DFT calculations were carried out using the slab-supercell approach, with the Vienna Ab-initio Simulation Package (for further details, see **Section 9B** in the **SI**). The MgO(100) surface has been modeled with (2×2) periodicity and a three-layers slab with eight Mg and O atoms per layer. As for the interaction with Cu with the MgO surface, it was considered that Cu species may dope the MgO surface or adsorb on it. Moreover, the Cu_2O(110) surface was modeled with (1 x 1) periodicity and a Cu_2O slab consisting of 6 alternating Cu−O and Cu layers. A full monolayer adsorption (saturation coverage) of CO molecules on these surfaces was considered and vibrational spectra were calculated. Moreover, the stability and vibrational spectra of differently coordinated formate species on hydroxylated undoped and Cu-doped MgO(100) surfaces have been assessed.

- **RESULTS AND DISCUSSION**

Synthesis, characterization and catalytic properties of calcined-reduced catalysts

Two Cu-Mg-Al mixed oxide catalysts containing 10 wt% Cu have been prepared starting from a Cu-Mg-Al hydrotalcite (HT) precursor (details in the **Experimental section**). In this study, the molar ratio $Cu^{2+}/Mg^{2+}/Al^{3+}$ has been fixed to 6/74/20, which, based on our previous work,[26] results in materials of large surface area (S_{BET} ~200 m^2/g), exhibiting high metal dispersion and moderate basic sites. These features, that are critical for an enhanced CO_2 hydrogenation activity and methanol selectivity, are found in the range of previously reported catalysts[24,34] and that of a commercial like $Cu/ZnO/Al_2O_3$ sample synthetized as reference catalyst (see **Section 4** and **5** of **SI**). The co-precipitated Cu-Mg-Al-hydrotalcite catalysts were first calcined at 550 °C under an air atmosphere, and then reduced in H_2 at two temperatures: 230 and 450 °C. After this procedure, two ex-solved copper-based systems are obtained, labelled as CuHT-230 and CuHT-450, respectively.

The catalysts properties derived from physico-chemical characterization techniques are included in **Table 1** (together with those of other reference samples) and discussed in the **SI**.

Catalyst	M^{II}/M^{III} (mol.ratio)[a]	Mg/Al (wt.%)	Cu content[a] (wt.%)	Surface area ($m^2 \cdot g_{cat}^{-1}$)[b]	Particle size (nm)[d]	Cu exp. area ($m^2_{Cu} \cdot g_{cat}^{-1}$) [$g_{Cu} \cdot g_{cat}^{-1}$)[h]
CuHT-230	4.1	40.1/11.7	9.4	180	1.9	35.7 [$5.5 \cdot 10^{-2}$]
CuHT-450	4.1	40.1/11.7	9.4	180	2.3	29.8 [$4.6 \cdot 10^{-2}$]
Cu/HT (w)	4.1	33.7/10.0	8.8	169	2.3[e]	26.0 [$4.0 \cdot 10^{-2}$]
Cu/HT (ACN)	4.4	28.3/7.8	7.1	147	*n/d*	-
$Cu/(Al_2O_3/MgO)$	3.6	38.8/13.0	8.3	144	2.6[f]	19.1 [$2.9 \cdot 10^{-2}$]
Cu/SiO_2	-	-	1.5	162[c]	3.3[g]	-

Table 1. Main physico-chemical properties of Cu-based materials.

[a]Measured by ICP. [b]Values calculated from the N_2 adsorption isotherm by applying the BET method. [c]Surface area of the bare support. [d]Average Cu particle size by HR-TEM with the σ value (a minimum of 200 particles was considered) for the reduced material. [e]Considering >60% particles (see SI). [f]Considering >70% particles (see SI). [g]Considering >90% particles (see SI).[h] Cu surface area determined by N_2O and mass of exposed copper in $g_{Cu} \cdot g_{cat}^{-1}$ [in square brackets].

XRD provides convincing proof of the formation of the desired hydrotalcite phase in the as-prepared samples and the corresponding mixed metal oxide in the calcined and reduced samples (see **Figure S2**, **SI**). Diffraction peaks associated with other phases (like $MgAl_2O_4$ spinel or Al_2O_3) or copper related species are not detected, suggesting a high copper dispersion in the samples. Indeed, in the reduced samples, the ex-solution of small and narrowly distributed Cu NPs with a particle size of ~2.0 nm has been confirmed by high-resolution transmission electron microscopy (HR-TEM), independently of the reduction temperature, ascertaining a remarkable

stability of the so formed Cu NPs (**Figure 1**). Elemental EDS analyses were used to properly distinguish Cu NPs from the support (see **Figure S5b**).

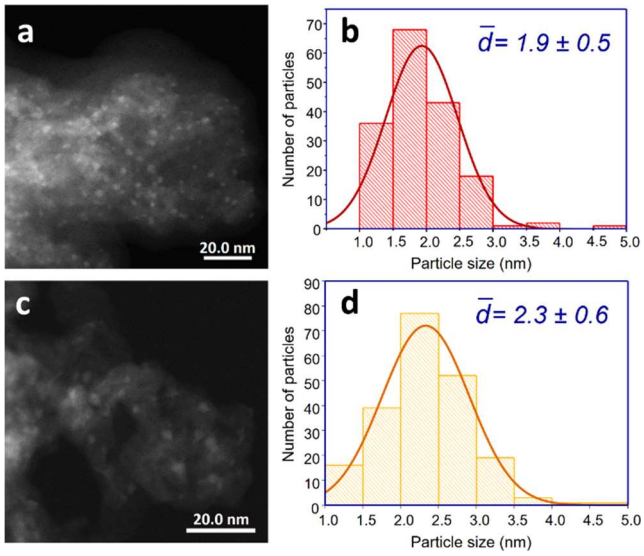

Figure 1. Left, HR-TEM images of CuHT-230 (a) and CuHT-450 catalysts (c). Right, particle size distribution for CuHT-230 (b) and CuHT-450 catalysts (d). More than 200 particles have been measured in each sample.

It has been reported that nano-sized copper NPs (<4 nm), supported on non-redox supports and in the absence of promoters, result in low methanol formation.[9-14] This behaviour is not observed in our study (**Table S1-S3**). In particular, the methanol yield at 230 °C, 20 bar and WHSV of ~28500 $mL \cdot g_{cat} \cdot h^{-1}$ over the CuHT-230 catalyst is $2.6 \cdot 10^{-3}$ $mol_{MeOH} \cdot g_{cat}^{-1} \cdot h^{-1}$, which normalized by the amount of exposed copper determined by N_2O titration ($5.5 \cdot 10^{-2}$ $g_{Cu} \cdot g_{cat}^{-1}$, see Table 1) results in $4.7 \cdot 10^{-2}$ $mol_{MeOH} \cdot g_{Cu}^{-1} \cdot h^{-1}$ with 71% methanol selectivity (**Table S2**). This value surpasses that of a previously reported $Cu/MgO/Al_2O_3$ catalyst,[13] where 8.2 $mg_{MeOH} \cdot mL_{cat}^{-1} \cdot h^{-1}$ ($5.1 \cdot 10^{-4}$ $mol_{MeOH} \cdot g_{cat}^{-1} \cdot h^{-1}$) at 20 bar, 200 °C and GHSV of 2000 h^{-1} has been found. Moreover, the catalytic activity of the herein reported CuHT-derived catalysts outperforms that referred in the literature with similar particle size (**Figure S11**), and the $Cu\text{-}Me@SiO_2$ promoted catalysts reported by Copéret et al,[18,19] when working at high contact time. In opposition to these previously reported catalysts, the ones in this study do not need expensive promoters or a complicated air sensitive synthesis methodology, thus leading to promising cost-efficient catalysts.

In order to figure out if the hydrotalcite precursor plays a critical role in the catalytic performance of the final material, an alternative $Cu/(Al_2O_3/MgO)$ catalyst was prepared. In this case, the support does not derive from a HT precursor, although displaying similar acid-base properties as the HT-derived catalyst (**Figure S10b**). In this sample, copper has been added using the incipient wetness impregnation methodology onto an Al_2O_3/MgO support, resulting in a

heterogeneous particle size distribution, with most particles around 2.6 nm (**Figure S8**). Using the same synthetic approach, two Cu impregnated Mg-Al HT catalysts (Cu/HT (w) and Cu/HT (ACN), where "w" and "ACN" denote impregnation in either water or acetonitrile) have also been prepared (**Figure S7**), resulting in similar particle size distributions as the Cu/(Al_2O_3/MgO) sample. Finally, the performance of these catalysts in the CO_2 hydrogenation has been compared to that of a Cu/SiO_2 catalyst of 3.3 nm particle size (**Figure S9**), prepared as in Refs (31,35-36). More details are in the **Experimental Section** and **Table 1**.

As shown in **Figure 2,** and according to the data in **Table S2**, the methanol yield (STY) increases in the order Cu/SiO_2 < Cu/(Al_2O_3/MgO) << CuHT-450 < Cu/HT (ACN) ~ Cu/HT (w) < CuHT-230. Notoriously, all HT-based samples show significantly higher methanol production than the other catalysts, independently of the more heterogeneous particle size distribution in the impregnated samples, this highlighting the positive role of the HT-type precursor.

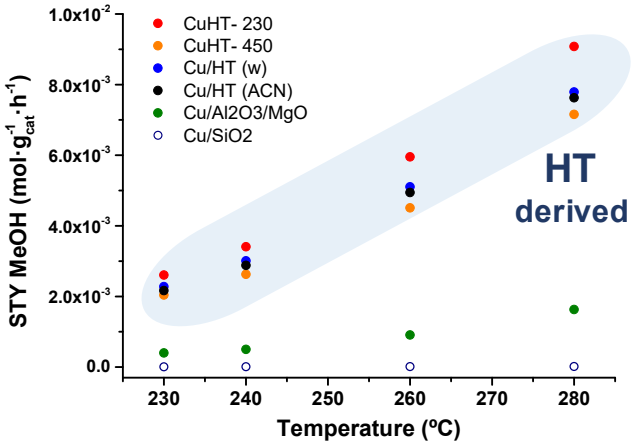

Figure 2. Methanol productivity of studied Cu based samples at variable temperature and 20 bar pressure (3:1 H_2/CO_2 vol% ratio, WHSV ~28500 mL·g_{cat}^{-1}·h^{-1}).

The effect of the contact time on the catalytic activity and selectivity has been studied (details in **Table S3**) on three selected samples (CuHT-230, Cu/(Al_2O_3/MgO), and Cu/SiO_2), where the variation of the selectivity to methanol with the CO_2 conversion obtained at 230 °C is given in **Figure 3a**. A higher selectivity is observed in the CuHT-230 catalyst, with a methanol selectivity around 67-70% at conversions < 22%, while it is lower in the case of Cu/(Al_2O_3/MgO) and Cu/SiO_2 samples (i.e., 50-57% and 5-8%, respectively). Interestingly, the CuHT-230 sample maintains remarkable methanol selectivity when the CO_2 conversion is increased up to the equilibrium level (i.e. ~22%), behaviour not common in conventional based Cu/ZnO samples, where the methanol selectivity tends to drop with the conversion (**Figure 3b**). displaying competitive methanol selectivity with respect to the commercial Cu/ZnO/Al_2O_3, at the same level of conversion (15% and 20%).

Analysing the initial formation rates of methanol and CO (obtained by extrapolating the respective rates to zero contact time, **Figure S12**), both CO and methanol appear as primary products in all three catalysts (**Figure 3c**). In the CuHT-230 catalyst, methanol formation is favoured over CO formation. In contrast, CO predominates over methanol formation with Cu/(Al_2O_3/MgO) and particularly with the Cu/SiO_2 catalyst. This last behaviour has been reported for non-promoted nano-sized Cu catalysts, being more active for the RWGS than for methanol synthesis.[11,37,38] According to this, the opposite trend observed in the CuHT-230 sample may indicate a different active site state, as determined later.

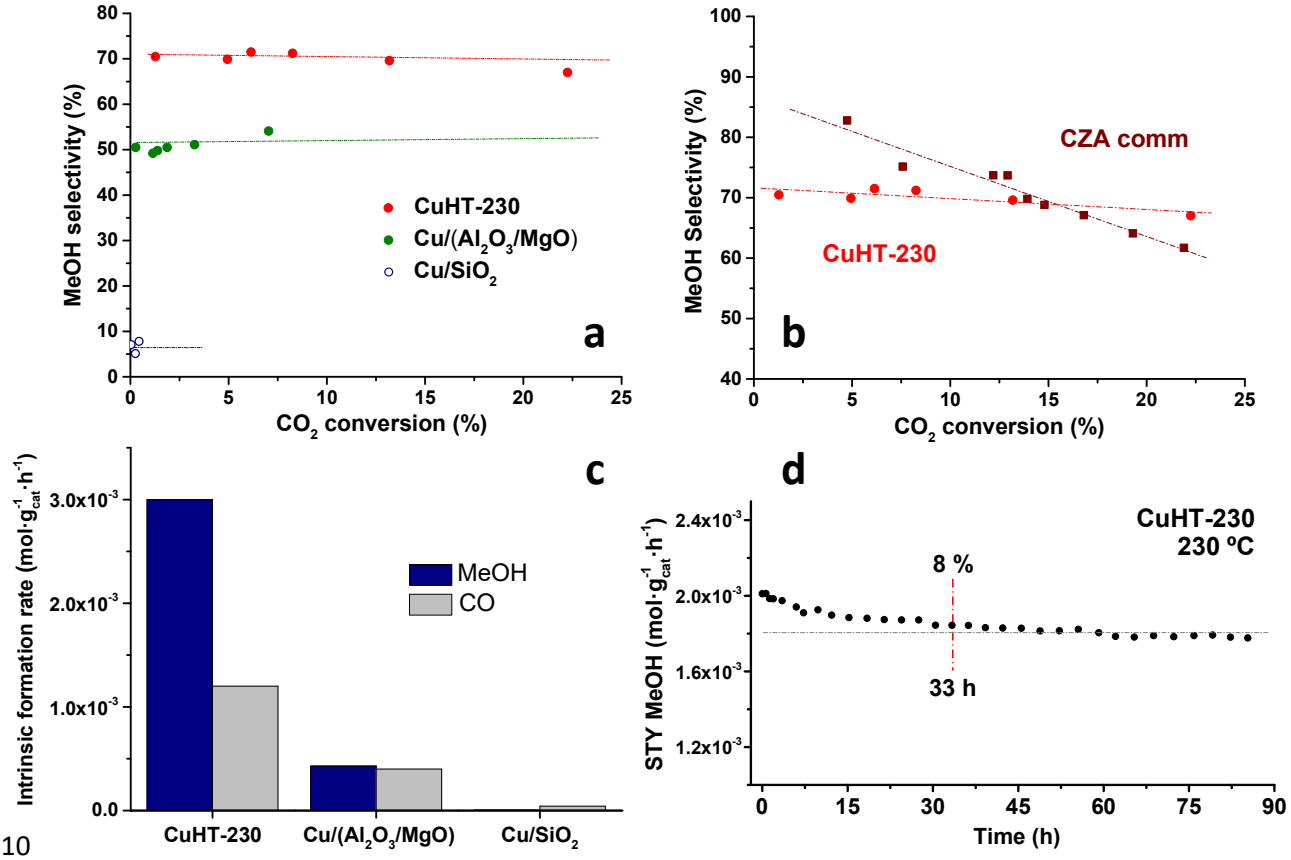

Figure 3. Variation of the MeOH selectivity versus CO_2 conversion at 230 °C and 20 bar on samples under study (a) and comparison between a commercial Cu/ZnO/Al_2O_3 catalyst (CZA comm) and the CuHT-230 sample under the same catalytic conditions (b). CZA comm was prepared according to the work of Baltes *et al.*[39] Intrinsic formation rates of methanol and CO for representative catalytic systems (c). Long-term stability of CuHT-230 system at 230 °C, 20 bar and 5700 mL·g_{cat}^{-1}·h^{-1} (d).

In catalysts for methanol synthesis, long-term and thermal stability are crucial for practical applications. Significantly, the CuHT-230 catalyst shows high long-term stability with more than 85 h of time of stream (TOS) (**Figure 3d**) operating at 20 bar, 230 °C, and 5700 mL·g_{cat}^{-1}·h^{-1}. An

initial decrease in methanol formation (8%) is observed during the first ~33 h, then remaining stable until the end of the experiment. It is worth noting that conventional Cu-based catalysts in the absence of Al_2O_3 as stabilizer tend to deactivate when operating at high temperatures (280-300 °C). In contrast, the CuHT-230 catalyst displays high thermal resistance against alternating cycles of temperatures between 230 and 280 °C (**Figure S13B**), without apparent deactivation.

In this direction, the stability of the CuNPs in the HT-derived material has been studied by HR-TEM of the spent catalyst (**Figure S14**), reflecting a change in the particle size from 1.9 to 3.2 after one catalytic cycle and then remaining quite stable reaching 4.1 nm after four high-temperature steps at 280 °C. Such particle stability is likely due to the stable ex-solution sites, at which the particles are tightly anchored.[40] Interestingly, lattice fringes corresponding to the laminar structure of the HT are observed in the CuHT-230 sample after being submitted to several cycles of temperature. This feature corresponds to the "HT-memory effect", a behaviour later discussed.

In order to understand the reason behind the outstanding activity of the herein Cu-HT derived samples, spectroscopic studies using surface sensitive tools (X-ray photoelectron spectroscopy (XPS) and operando Infrared (IR) - mass spectrometry (MS)) studies combined with IR-CO titration experiments have been performed.

Spectroscopic catalyst characterization.

The chemical state of the Cu NPs has been studied by XPS and IR of CO. XPS spectra show the presence of Cu^0 in all reduced samples, characterized by BE of ~932.5 eV at the Cu $2p_{3/2}$ core line and a Cu L_3VV auger peak maxima at around 918.4 eV KE (**Figure S15** and **Table S4-S6**). From XPS and the auger peak the presence of minority Cu^+ species are hard to detect. However, by IR spectroscopy using CO as probe molecule, a higher surface sensitivity is obtained, and Cu^+ species (IR band at 2138-2135 cm^{-1}) together with Cu^0 (IR bands at 2100-1990 cm^{-1}) and Lewis acid sites and OH groups of the support (~2168 and ~2150 cm^{-1}) are observed on reduced samples (**Figure 4**).[41-43] The amount of Cu^+ in the HT-derived samples follows the order CuHT-230 ≥ CuHT-450 >> Cu/HT (w) ~ Cu/HT (ACN) (**Figure 4e**), being absent in the Cu/(Al_2O_3/MgO) and Cu/SiO_2 samples (**Figure S18**). (More details in **SI, Section 8**). Interestingly, Cu^+ ions are unexpectedly observed in the Cu/HT (w) sample, prepared by impregnation of a calcined Mg-Al HT support with an aqueous solution of a copper salt. It is known that the presence of water promotes the so-called "HT-memory effect" (as observed in the XRD pattern of **Figure S4**), favouring the relocation of $Cu^{2+/+}$ ions in lattice positions.[44] Especially, it has been reported that

the reconstruction of the hydrotalcite structure has a beneficial effect on maximizing the Cu^{+}/Cu^{0} ratio in the corresponding reduced materials.[45] Indeed, even when performing the same impregnation procedure with an organic solution using acetonitrile, a reversion toward the HT structure is again detected from the XRD pattern, although to less extent, together with the stabilization of lattice Cu^{+} ions in the IR-CO spectra.

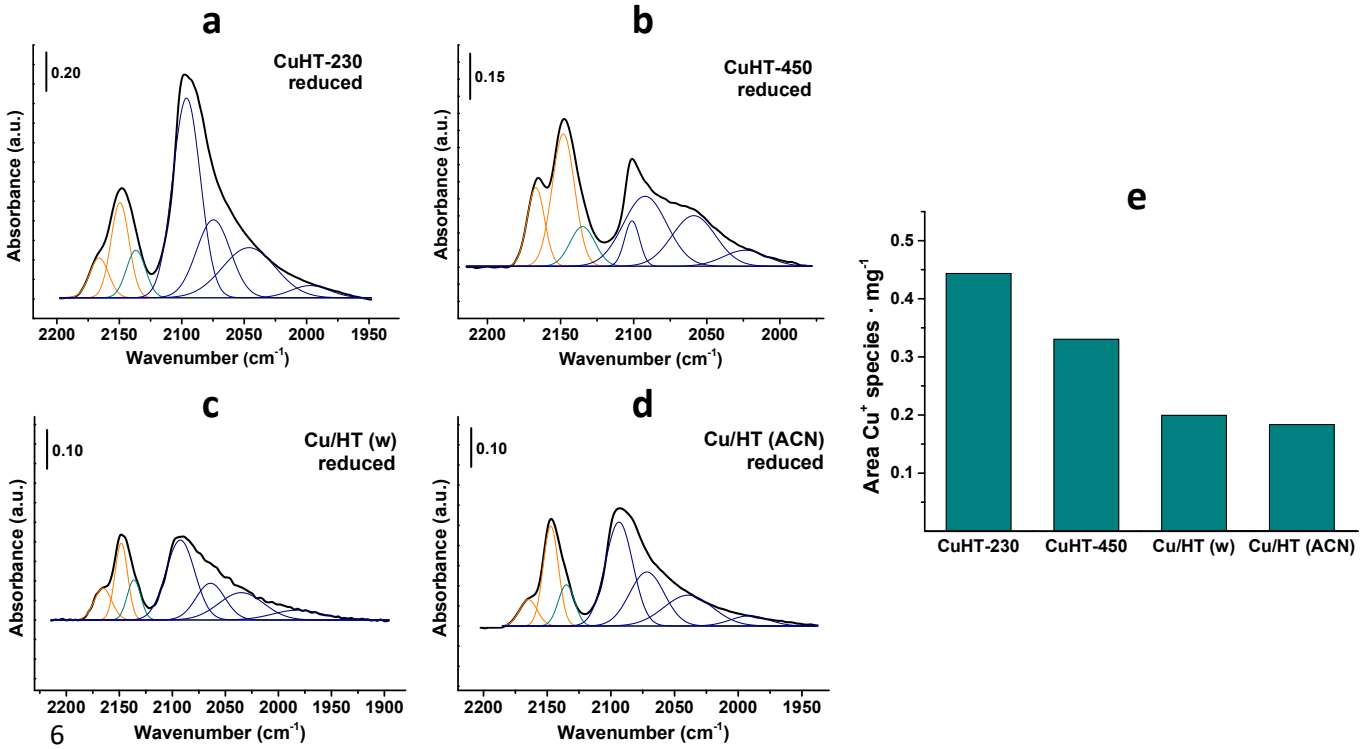

Figure 4. IR of CO adsorption at -170 °C and saturation coverage on reduced CuHT-derived samples: a) CuHT-230, b) CuHT-450, c) Cu/HT (w), d) Cu/HT (ACN). Color code for deconvoluted components: orange (HT support), dark cyan (Cu^{+} species), navy (Cu^{0} species). e) Comparison between the amount of Cu^{+} species normalized to sample weight analyzed at saturation coverage.

Concerning the nature of Cu^{+} ions, a detailed analysis of the IR data, supported by DFT simulations and combined with UV-VIS studies allows for assigning the IR band at ≈2137 cm^{-1} to highly dispersed Cu^{+} ions in metal oxide lattice positions. Indeed, when CO interacts with Cu_2O, its frequency appears around 2118-2127 cm^{-1},[41,46-49] while when it coordinates with isolated Cu^{+} ions it has been reported at 2137 cm^{-1}.[50-52] Similar shifts in the CO frequencies with respect to the gas phase molecule have been retrieved from the DFT simulations (see **Section 9** in the **SI**), where the IR band at 2137 cm^{-1} has been correlated to dopant Cu ions in the metal oxide lattice. In addition, the presence of isolated Cu^{2+} and Cu^{+} ions in the metal oxide lattice is confirmed by diffuse reflectance UV-VIS analysis (bands at 265 and 227 nm, respectively, see **Figure S19**) being

the amount of Cu^+ ions enhanced in the reduced CuHT-230 sample. In conclusion, the above reported results reveal the coexistence of Cu NPs and Cu^+ ions likely located in lattice positions of the reduced HT-derived mixed oxide catalysts. The fact that Cu^+ ions are only observed in the HT-derived samples and not in the Cu/(Al_2O_3/MgO) or Cu/SiO_2 samples could explain the different catalytic performance of the materials, considering that Cu^+ has been reported in several works to enhance methanol production.[12,53,54]

It must be highlighted that water is formed under reaction conditions and, as indicated above, water promotes the reconstruction of the metal oxide structure allowing relocation of Cu^+ ions in lattice positions. At the same time, it may also behave as an oxidant competing with the reducing effect of H_2 in the reaction feed or even assisting the desorption of the so-formed methanol or methoxy species during reaction. Thus, it is not surprising that the reaction conditions (as the reaction pressure) strongly influence the identification of copper species (Cu^0, Cu_2O, CuO) as well as the stabilization of lattice Cu^+ ions, behaviour confirmed from operando spectroscopic studies, as detailed in the next section.

Operando spectroscopic studies combined with titration studies

From IR studies, significant transformations are identified on the catalyst surface depending on the working pressure. This is revealed on the quenched sample after 2 h of reaction at 230 °C and 1 or 9 bar, submitted to CO titration at low temperature (-170 °C) (see **Experimental Section** for more details). For instance, while similar trends are observed in all samples, titration experiments performed on the most active CuHT-230 sample after reaction at 1 bar reveal slight oxidation of the copper nanoparticles with the formation of surface Cu_2O species, whereas at 9 bar the copper nanoparticles appear fully reduced (**Figure S22**). In addition, compared to the reduced catalyst, a decrease in the IR band ascribed to Cu^0 sites, especially those appearing at lower ν(C≡O) frequencies, is observed at both pressures. This decrease is due to the poisoning of the copper surface by reaction products, as will be demonstrated later. Simultaneously, an increase in surface doped Cu^+ ions (IR band at ~2137 cm^{-1}) is detected. This is particularly observed when working at 9 bar, (**Figures S23-24**), and it is linked to the higher reactivity of the samples (and, accordingly, water formation) at increasing reaction pressure. This higher reactivity is confirmed by online MS analysis and is aligned with catalytic studies performed at different pressures (**Figure S25**).

In the next, considering all samples studied in this work, we calculated the concentration of Cu^0 and surface doped Cu^+ sites, before and after operando IR reaction at 9 bar, which is given in **Figure 5** (the corresponding spectra and their respective deconvolution are shown in **Figure 4, and Figure S23**). In particular, the concentration of Cu^+ after reaction increases in all CuHT

samples (**Figure 5a**), reaching a final value of 0.55-0.65 in all of them. In addition, a decrease in the Cu^0 sites is observed in all samples (**Figure 5b**), being ~70% in the CuHT-230 sample, for instance.

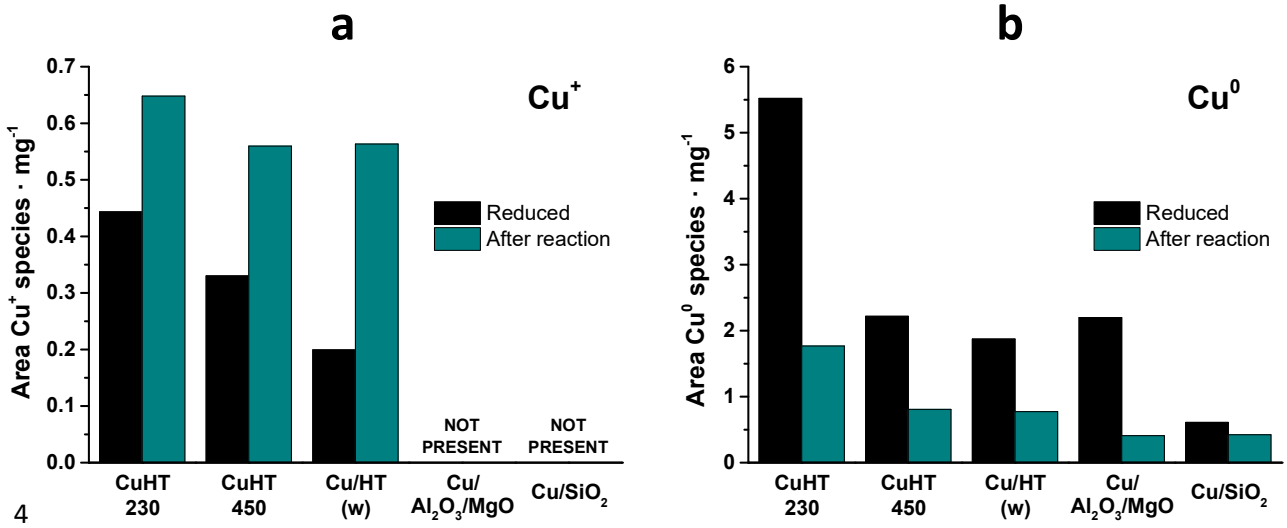

Figure 5. Normalized area of the IR component associated to CO coordinated to Cu^+ (IR band at ~2137 cm^{-1}) (a); and Cu^0 (IR bands between 2115-1990 cm^{-1}) (b); before (i.e., reduced samples) and after CO_2 hydrogenation at 9 bar.

In order to establish structure-activity correlations and identify the nature of the active sites, IR data of the IR-CO titration experiments after operando IR reaction at 9 bar have been compared with the catalytic performance of the samples in the fixed bed reactor. On the one hand, the amount of unblocked Cu^0 sites has been correlated with catalytic activity and/or selectivity. In general, it is widely accepted that Cu^0 sites are needed for CO_2 hydrogenation,[55-59] in particular for H_2 dissociation. Some authors reported a linear relationship[11,25,33] between the methanol yield and the copper surface area, while other studies did not convey such a linear correlation [18,36,60] and in other cases metallic copper has been associated to the RWGS reaction.[61] In our case, we do not find a clear correlation between the amount of Cu^0 and the CO or methanol production (**Figure S26**). In contrast, when representing the amount of surface doped Cu^+ species under operando IR conditions at 9bar and the methanol yield (STY), a good linear correlation is obtained despite the pressure gap (**Figure 6**), thus highlighting the positive role of Cu^+ in methanol production. In definitive, while Cu^0 is necessary for catalytic activity, the controlling step in methanol production is determined by the presence of Cu^+ sites in the mixed metal oxide surface.

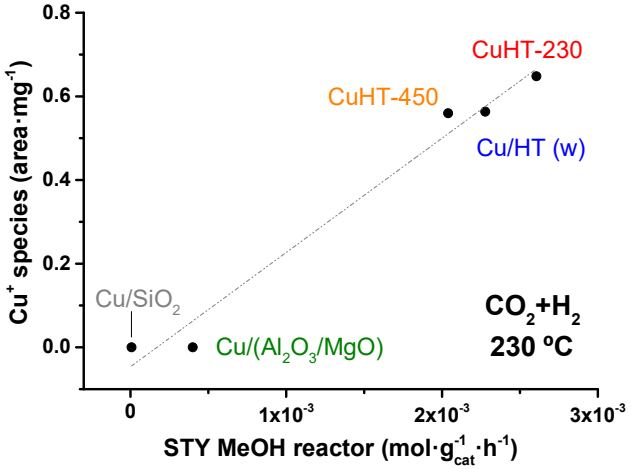

Figure 6. Correlation between methanol production at 20 bar in a fixed bed reactor (STY MeOH) and the amount of Cu^+ normalized to sample weight obtained in the operando IR studies at 9 bar.

Going one step further and aiming to gain mechanistic insights into the type of intermediate reaction species involved in the CO_2 hydrogenation reaction and the role of Cu^+ in the reaction mechanism, temperature resolved IR-MS studies have been done. In these experiments, the evolution of surface species in the IR spectra and the reaction products analysed by on-line MS are monitored on the most active CuHT-230 sample.

Working at 9 bar and in the temperature range from 160 to 230 °C, a complex set of IR bands growing in intensity in the 1670-1200 cm^{-1} region, associated with the contribution of different types of carbonate and formate species, are observed. Thus, IR bands[62-67] due to monodentate (*m*) formate (ν_{as}(OCO) 1670-1650 cm^{-1}, δ(C-H) 1355-1340 cm^{-1}, ν_s(OCO) 1310-1300 cm^{-1}); bridge (*b*) formate (ν_{as}(OCO) 1587-1579 cm^{-1}, δ(C-H) 1398-1395 cm^{-1}, ν_s(OCO) 1374-1369 cm^{-1}); bidentate carbonate (ν_{as}(OCO) 1536-1524 cm^{-1}, ν_s(OCO) 1330-1327 cm^{-1}); and bicarbonate species (ν_{as}(OCO) 1638-1621 cm^{-1}, ν_s(OCO) 1442-1440 cm^{-1}, δ(OH) 1248-1237 cm^{-1}) are observed. Cu^0 bonded formate (characterized by an IR band at 1350 cm^{-1}) and methoxy species (ν(C-O) 1087-1080 cm^{-1}) are also detected (**Figure S27**). At this point, identifying kinetically relevant intermediate species is challenging since no correlation between the MS and a parallel disappearance in the IR bands could be detected. This may be caused by the high working pressure, which enhances the rate of the sequential reaction steps and, accordingly, inhibits the detection of short-lived intermediate species. In fact, by performing isotopic studies replacing part of the H_2 flow by D_2 under steady-state conditions at 230 °C and 9 bar, the whole set of IR bands in the 1670-1200 cm^{-1} remain unaltered, and only the detection of OD bands (2630 cm^{-1}), and a very weak IR band at 1019 cm^{-1}, associated to δ (C-D) vibration, are observed (**Figure S28**).

Based on these results, it becomes evident that most of the identified IR species are not directly involved in the reaction mechanism, behaving as spectators, and blocking active sites of the copper surface, as described above. Further confirmation has been attained, by exposing the sample after IR operando conditions (i.e., in a CO_2/H_2 flow at 9 or 1 bar and 230 °C) to a H_2/N_2 flow at 230 °C during 4.5 h, followed by a subsequent IR-CO titration experiment. As shown in **Figure S29**, the intensity of the Cu^0-CO signal is restored, confirming that most of these species are blocking the copper surface under reaction conditions. Interestingly, hydrogenation of those adsorbed species results in CH_4 and CO formation, disregarding them as intermediate species in the methanol synthesis and behaving mostly as spectators (**Figure S30**). Remarkably, the poisoning of the Cu surface by a high surface coverage of adsorbed species has been reported by other authors as one of the reasons causing the low activity of small Cu NPs.[68]

Therefore, with the aim of slowing down the reaction kinetics, operando IR studies at lower pressure (i.e., 1 bar) have been carried out. At these conditions and through temperature resolved IR-MS experiments, accurate identification of reaction intermediate species in methanol, methane and CO formation is attained (**Figure 7**). Thus, by increasing the temperature from 160 to 200 °C, the disappearance of IR bands at 2934, 1660, 1348, and 1319 cm^{-1}, associated with $\nu_{stretch}$(C-H), ν_{as}(OCO), δ(C-H) and ν_s(OCO) vibrations of monodentate (*m*)-formate species,[64,66,69] respectively, parallels with the exclusive detection of methanol in the MS (**Figure 7** and **Figure S31**). A concomitant vanishing of the IR bands at 2853 and 1350 cm^{-1} assigned to formate species on the copper surface[70] is also observed, whereas its participation in the reaction can be ruled out.[69] A further increase in the reaction temperature to 230 °C results in the disappearance of additional IR bands at around 2872, 1578, 1397, and 1370 cm^{-1}, associated with the $\nu_{stretch}$(C-H), ν_{as}(OCO), δ(C-H) and ν_s(OCO) vibrations of bridge (*b*)-formate species, respectively, paralleling the detection of methane and CO in the MS and confirmed by GC analysis (**Figure 7** and **S32**). Assignation of both formate species is supported by their dissimilar $\Delta\nu_{as\text{-}s}$(OCO) splitting, i.e., 341 cm^{-1} for monodentate and 208 cm^{-1} of bridge formate species.[71] Using DFT analysis, we studied the stability and vibrational frequencies of differently coordinated formate species on modelled hydroxylated undoped and Cu^+-doped MgO(100) surfaces (more details in **Section 11** in the **SI**), and found that on the former bridge-type species are more stable ($\Delta\nu_{as\text{-}s}$(OCO) of 242 cm^{-1}), whereas on the latter, monodentate formate species stabilized on Cu^+ are favored ($\Delta\nu_{as\text{-}s}$(OCO) between 267-305 cm^{-1}), supporting the role of Cu^+ in the stabilization of monodentate formate species.

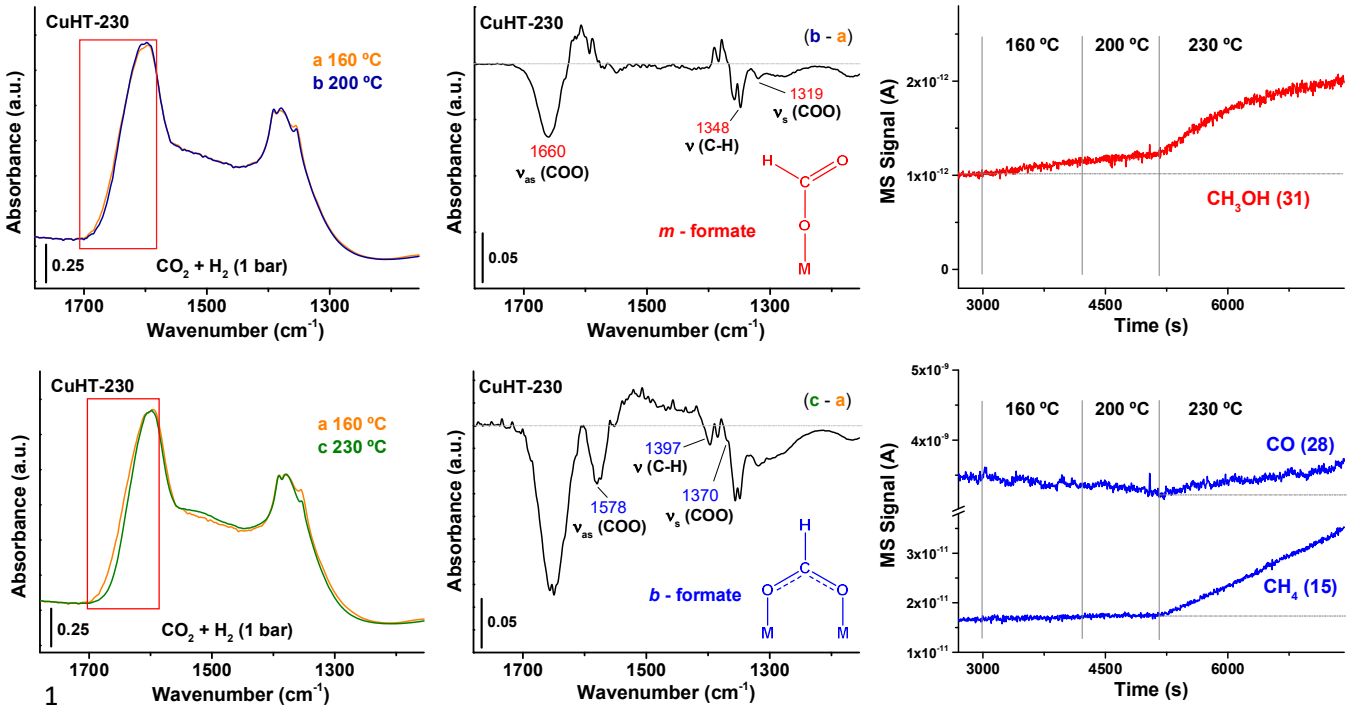

Figure 7. Temperature resolved IR studies under operando conditions at 1 bar in CO_2/H_2 flow. Left: IR spectra at specific temperature; Middle: subtracted spectra; Right: evolved reaction products detected by online MS.

These findings allow us to associate monodentate (*m*)-formate and bridge (*b*)-formate species as intermediate in methanol and methane/CO formation, respectively. These correlations have been controversially discussed previously in the literature and scarcely supported experimentally. Moreover, the earlier detection of methanol (onset temperature of 160 °C) in comparison to methane and CO (onset temperature of 230 °C) sustains the higher reactivity of *m*-formate species, in agreement with previous literature studies.[62,72]

Based on the previous spectroscopic and catalytic results, the unusual activity of the Cu-based HT-derived catalysts has been associated with the stabilization of lattice Cu^+ species. Accordingly, we can designate surface doped Cu^+ an active site in methanol formation, enabling the stabilization of *m*-formate intermediate species.

▪ CONCLUSIONS

In our work, a copper-based catalyst, mainly composed of inexpensive earth abundant MgO, prepared by an easy synthetic procedure and in the absence of promoters, has demonstrated

to be an interesting candidate for the CO_2 hydrogenation to methanol. The herein reported Cu mixed oxide catalyst derives from calcination and further reduction of an Mg-Al-Cu hydrotalcite precursor. The striking activity of the CuHT catalysts compared to conventional $Cu/Al_2O_3/MgO$ catalysts has been ascribed to the stabilization of Cu^+ ions in lattice positions. This stabilization seems to be promoted under reaction conditions, which results in partial reconstruction of the metal oxide lattice linked to the "HT-memory effect" in the presence of water. This feature confers high resistance to the catalyst during alternative sequential temperature cycles, overcoming usual deactivation, one of the most critical drawbacks in methanol synthesis *via* CO_2 hydrogenation. Operando temperature resolved IR-MS experiments have enabled the discernment of monodentate formate species as the intermediate in methanol synthesis. These monodentate formate species are much more reactive than bridge formate species, behaving the last ones as intermediates in methane and CO formation. Combining spectroscopic with catalytic studies, together with DFT calculations, the herein detected monodentate formate species are ascribed to surface doped Cu^+ ions, thereby explaining the remarked catalytic activity of the Cu-based HT-derived materials. In addition, other essential aspects that have remained ambiguous in the literature have been clarified in this study. Thus, high coverage of adsorbed species blocking preferentially low coordinated sites in the CuNPs has been visualized. Especially predominant in small Cu nanoparticles, these species behave mostly as non-intermediates species (i.e., spectators), whose hydrogenation results in methane and CO formation.

In conclusion, our work represents a step further in unraveling fundamental aspects that could help in the design of a new generation of efficient catalysts for CO_2 valorization.

▪ AUTHOR INFORMATION

Corresponding authors

*pconcepc@upvnet.upv.es

ORCID

Jorge Cored: 0000-0003-4223-270X

Jaime Mazarío: 0000-0002-1746-4552

Cristina Cerdá-Moreno: 0000-0001-5927-4055

Pablo G. Lustemberg: 0000-0003-4058-4023

M. Verónica Ganduglia-Pirovano: 0000-0003-2408-8898

Marcelo E. Domine: 0000-0002-1111-2855

Patricia Concepción: 0000-0003-2058-3103

Notes

The authors declare no competing financial interest.

▪ ASSOCIATED CONTENT

Supporting Information includes physico-chemical properties of the catalysts; State of the art in methanol synthesis; CO_2 hydrogenation catalytic results; Laboratory scale XPS studies; IR-CO and IR-CD_3CN titration experiment after different reaction conditions; UV-VIS analysis and DFT studies; Operando IR studies; Deuterated IR experiment; Hydrogenation treatment of spent CuHT-230. This information is available free of charge on the ACS Publications website.

▪ ACKNOWLEDGMENTS

The research leading to these results has received funding from the Spanish Ministry of Science, Innovation and Universities through "Severo Ochoa" Excellence Programme (SEV-2016-0683) and through the RTI2018-099668-B-C21 and RTI2018-101604-B-I00 projects. The authors also thank the Microscopy Service of UPV for kind help on measurements. J.C. thanks the Spanish Government (MINECO) for a "Severo Ochoa" grant (BES-2015-075748). J.M. thanks the MICINN (CTQ2015-67592) for his PhD scholarship. M.E.D. thanks financial support by Spanish Government (PGC2018-097277-B100). P.G. L. thanks the CSIC for the extension of the MSCA-IF Grant Agreement No. 832121. Computer time provided by the RES (Red Española de Supercomputación) resources at Mare Nostrum 4 (BSC, Barcelona) and La Palma (IAC, La Palma) nodes is acknowledged.

▪ REFERENCES

1. Ye, R. P.; Ding, J.; Gong, W.; Argyle, M. D.; Zhong, Q.; Wang, Y.; Russell, C. K.; Xu, Z.; Russell, A. G.; Li, Q.; Fan, M.; Yao, Y. G. CO_2 hydrogenation to high-value products via heterogeneous catalysis. *Nat. Commun.* **2019**, *10*, 5698. DOI: 10.1038/s41467-019-136389.
2. Centi, G.; Quadrelli, E. A.; Perathoner, S. Catalysis for CO_2 conversion: a key technology for rapid introduction of renewable energy in the value chain of chemical industries. *Energy Environ. Sci.* **2013**, *6*, 1711-1731. DOI: 10.1039/C3EE00056G.

3. Roy, S.; Cherevotan, A.; Peter, S. C. Thermochemical CO_2 Hydrogenation to Single Carbon Products: Scientific and Technological Challenges. *ACS Energy Lett.* **2018**, *3*, 1938-1966. DOI: 10.1021/acsenergylett.8b00740.
4. Grim, R. G.; Huang, Z.; Guarnieri, M. T.; Ferrell, J. R.; Tao, L.; Schaidle, J. A. Transforming the carbon economy: challenges and opportunities in the convergence of low-cost electricity and reductive CO_2 utilization. *Energy Environ. Sci.* **2020**, *13*, 472-494. DOI: 10.1039/C9EE02410G.
5. Kajaste, R.; Hurme, M.; Oinas, P. Methanol-Managing greenhouse gas emissions in the production chain by optimizing the resource base. *AIMS Energy* **2018**, *6*, 1074-1102. DOI: 10.3934/energy.2018.6.1074.
6. Sheldon, D. Methanol Production – A Technical History. *Johnson Matthey Technol. Rev.* **2017**, *61*, 172-182. DOI: 10.1595/205651317X695622.
7. Liu, L.; Corma, A. Metal Catalysts for Heterogeneous Catalysis: From Single Atoms to Nanoclusters and Nanoparticles. *Chem. Rev.* **2018**, *118*, 4981-5079. DOI: 10.1021/acs.chemrev.7b00776.
8. Van der Berg, R.; Prieto, G.; Korpershoek, G.; Van der Wal, L. I.; Van Bunningen, A. J.; Laegsgaard-Jorgensen, S.; De Jongh, P. E.; De Jong, K. P. Structure sensitivity of Cu and CuZn catalysts relevant to industrial methanol synthesis. *Nat. Commun.* **2016**, *7*, 13057. DOI: 10.1038/ncomms13057.
9. Yang, H.; Gao, P.; Zhang, C.; Zhong, L.; Li, X.; Wang, S.; Wang, H.; Wei, W.; Sun, Y. Core-shell structured Cu@m-SiO_2 and Cu/ZnO@m-SiO_2 catalysts for methanol synthesis from CO_2 hydrogenation. *Catal. Commun.* **2016**, *84*, 56-60. DOI: 10.1016/j.catcom.2016.06.010.
10. Wang, Z. Q.; Xu, Z. N.; Peng, S. Y.; Zhang, M. J.; Lu, G.; Chen, Q. S.; Chen, Y.; Guo, G. C. High-Performance and Long-Lived Cu/SiO_2 Nanocatalyst for CO_2 Hydrogenation. *ACS Catal.* **2015**, *5*, 4255-4259. DOI: 10.1021/acscatal.5b00682.
11. Karelovic, A.; Galdames, G.; Medina, J. C.; Yévenes, C.; Barra, Y.; Jiménez, R. Mechanism and structure sensitive of methanol synthesis from CO_2 over SiO_2-supported Cu nanoparticles. *J. Catal.* **2019**, *369*, 415-426. DOI: 10.1016/j.jcat.2018.11.012.
12. Yu, J.; Yang, M.; Zhang, J.; Ge, Q.; Zimina, A.; Pruessmann, T.; Zheng, L.; Grunwaldt, J. D.; Sun, J. Stabilizing Cu^+ in Cu/SiO_2 Catalysts with a Shattuckite-Like Structure Boosts CO_2 Hydrogenation into Methanol. *ACS Catal.* **2020**, *10*, 14694-14706. DOI: 10.1021/acscatal.0c04371.
13. Dasireddy, V. D. B. C.; Stenfancic, N. S.; Lizokar, B. Correlation between synthesis pH, structure and Cu/MgO/Al_2O_3 heterogeneous catalyst activity and selectivity in CO_2

hydrogenation to methanol. *J. CO_2 Util.* **2018**, *28*, 189-199. DOI: 10.1016/j.jcou.2018.09.002.

14. Liu, C.; Guo, X.; Guo, Q.; Mao, D.; Yu, J.; Lu, G. Methanol synthesis from CO_2 hydrogenation over copper catalysts supported in MgO-modified TiO_2. *J. Mol. Catal. A Chem.* **2016**, *425*, 86-93. DOI: 10.1016/j.molcata.2016.09.032.
15. Tada, S.; Otsuka, F.; Fujiwara, K.; Moularas, C.; Deligiannakis, Y.; Kinoshita, Y.; Uchida, S.; Honma, T.; Nishijima, M.; Kikuchi, R. Development of CO_2-to-Methanol Hydrogenation Catalyst by Focusing on the Coordination Structure of the Cu species in Spinel-Type Oxide $Mg_{1-x}Cu_xAl_2O_4$. *ACS Catal.* **2020**, *10*, 15186-15194. DOI: 10.1021/acscatal.0c02868.
16. Lam, E.; Larmier, K.; Wolf, P.; Tada, S.; Safonova, O. V.; Copéret, C. Isolated Zr Surface Sites on Silica Promote Hydrogenation of CO_2 to CH_3OH in Supported Cu Catalysts. *J. Am. Chem. Soc.* **2018**, *140*, 10530-10535. DOI: 10.1021/jacs.8b05595.
17. Noh, G.; Lam, E.; Alfke, J. L.; Larmier, K.; Searles, K.; Wolf, P.; Copéret, C. Selective Hydrogenation of CO_2 to CH_3OH on Supported Cu Nanoparticles Promoted by Isolated Ti^{IV} Surface Sites on SiO_2. *ChemSusChem*, **2019**, *12*, 968-972. DOI: 10.1002/cssc.201900134.
18. Lam, E.; Noh, G.; Chan, K. W.; Larmier, K.; Lebedev, D.; Searles, K.; Wolf, P.; Safonova, O. V.; Copéret, C. Enhanced CH_3OH selectivity in CO_2 hydrogenation using Cu-based catalysts generated *via* SOMC from Ga^{III} single-sites. Chem. *Sci.* **2020**, *11*, 7593-7598. DOI: 10.1039/D0SC00465K.
19. Lam, E.; Noh, G.; Larmier, K.; Safonova, O. V.; Copéret, C. CO_2 hydrogenation on Cu-catalysts generated from Zn^{II} single-sites: Enhanced CH_3OH selectivity compared to $Cu/ZnO/Al_2O_3$. *J. Catal.* **2021**, *394*, 266-272. DOI: 10.1016/j.jcat.2020.04.028.
20. Sels, B. F.; De Vos, D. E.; Jacobs, P. A. Hydrotalcite-like anionic clays in catalytic organic reactions. *Catal. Rev.* **2001**, *43*, 443-488. DOI: 10.1081/CR-120001809.
21. Dewangan, N.; Hui, W. M.; Jayaprakash, S.; Bawah, A. R.; Poerjoto, A. J.; Jie, T.; Jangam, A.; Hidajat, K.; Kawi, S. Recent progress on layered double hydroxide (LDH) derived metal-based catalysts for CO_2 conversion to valuable chemicals. *Catal. Today* **2020**, *356*, 490-513. DOI: 10.1016/j.cattod.2020.06.020.
22. Fang, X.; Chen, C.; Jia, H.; Li, Y.; Liu, J.; Wang, Y.; Song, Y.; Du, T.; Liu, L. Progress in Adsorption-Enhanced Hydrogenation of CO_2 on Layered Double Hydroxide (LDH) Derived Catalysts. *J. Ind. Eng. Chem.* **2021**, *95*, 16-27. DOI: 10.1016/j.jiec.2020.12.027.
23. Gao, P.; Li, F.; Xiao, F.; Zhao, N.; Sun, N.; Wei, W.; Zhong, L.; Sun, Y. Preparation and activity of Cu/Zn/Al/Zr catalysts *via* hydrotalcite-containing precursors for methanol synthesis from CO_2 hydrogenation. *Catal. Sci. Technol.* **2012**, *2*, 1447-1454. DOI: 10.1039/C2CY00481J.

24. Gao, P.; Li, F.; Zhan, H.; Zhao, N.; Xiao, F.; Wei, W.; Zhong, L.; Wang, H.; Sun, Y. Influence of Zr on the performance of Cu/Zn/Al/Zr catalysts via hydrotalcite-like precursors for CO_2 hydrogenation to methanol. *J. Catal.* **2013**, *298*, 51-60. DOI: 10.1016/j.jcat.2012.10.030.
25. Chen, Y.; Hong, H.; Cai, J.; Li, Z. Highly Efficient CO_2 to CO Transformation over Cu-Based Catalyst Derived from a CuMgAl-Layered Double Hydroxide (LDH). *Chem. Cat. Chem.* **2021**, *13*, 656-663. DOI: 10.1002/cctc.202001611.
26. Mazarío, J.; Concepción, P.; Ventura, M.; Domine, M. E. Continuous catalytic process for the selective dehydration of glycerol over Cu-based mixed oxide. *J. Catal.* **2020**, *385*, 160-175. DOI: 10.1016/j.jcat.2020.03.010.
27. Climent, M. J.; Corma, A.; De Frutos, P.; Iborra, S.; Noy, M.; Velty, A.; Concepción, P. Chemicals from biomass: Synthesis of glycerol carbonate by transesterification and carbonylation with urea with hydrotalcite catalysts. The role of acid-base pairs. *J. Catal.* **2010**, *269*, 140-149. DOI: 10.1016/j.jcat.2009.11.001.
28. Blanch-Raga, N.; Palomares, A. E.; Martínez-Triguero, J.; Fetter, G.; Bosch, P. Cu Mixed Oxides Based on Hydrotalcite-Like Compounds for the Oxidation of Trichloroethylene. *Ind. Eng. Chem. Res.* **2013**, *52*, 15772-15779. DOI: 10.1021/ie4024935.
29. Yaseneva, P.; An, N.; Finn, M.; Tiedemann, N.; Jose, N.; Voutchkova-Kostal, A.; Lapkin, A. Continuous synthesis of doped layered double hydroxides in a meso-scale flow reactor. *Chem. Eng. J.* **2019**, *360*, 190-199. DOI: 10.1016/j.cej.2018.11.197.
30. Dumitriu, E.; Hulea, V.; Chelaru, C.; Catrinescu, C.; Tichit, D.; Durand, R. Influence of the acid-base properties of solid catalysts derived from hydrotalcite-like compounds on the condensation of formaldehyde and acetaldehyde. *Appl. Catal. A-Gen.* **1999**, *178*, 145-157. DOI: 10.1016/S0926-860X(98)00282-8.
31. Stöber, W.; Fink, A.; Bohn, E. Controlled growth of monodisperse silica spheres in the micron size range. *J. Colloid Interface Sci.* **1968**, *26*, 62-69. DOI: 10.1016/0021-9797(68)90272-5.
32. Luo, W.; Jing, F. L.; Yu, X. P.; Sun, S.; Luo, S. Z.; Chu, W. Synthesis of 2-Methylpyrazine Over Highly Dispersed Copper Catalysts. *Catal. Lett.* **2012**, *142*, 492-500. DOI: 10.1007/s10562-012-0782-8.
33. Hinrichsen, O.; Genger, T.; Muhler, M. Chemisorption of N_2O and H_2 for the Surface Determination of Copper Catalysts. *Chem. Eng. Technol.* **2000**, *23*, 956-959. DOI: 10.1002/1521-4125(200011)23:11<956::AID-CEAT956>3.0.CO;2-L.
34. Frusteri, L.; Cannilla, C.; Todaro, S.; Frusteri, F.; Bonura, G. Tailoring of Hydrotalcite-Derived Cu-Based Catalysts for CO_2 Hydrogenation to Methanol. *Catalysts* **2019**, *9*, 1058. DOI: 10.3390/catal9121058.

35. Oliveira, R. L.; Kiyohara, P. K.; Rossi, L. M. High performance magnetic separation of gold nanoparticles for catalytic oxidation of alcohols. *Green Chem.* **2010**, *12*, 144-149. DOI: 10.1039/B916825G.
36. Jacinto, M. J.; Kiyohara, P. K.; Masunaga, S. H.; Jardim, R. F.; Rossi, L. M. Recoverable rhodium nanoparticles: Synthesis, characterization and catalytic performance in hydrogenation reactions. *Appl. Catal. A-Gen* **2008**, *338*, 52-57. DOI: 10.1016/j.apcata.2007.12.018.
37. Medina, J. C.; Figueroa, M.; Manrique, R.; Pereira, J. R.; Srinivasan, P. D.; Bravo-Suárez, J. J.; Baldovino-Medrano, V. G.; Jiménez, R.; Karelovic, A. Catalytic consequences of Ga promotion on Cu for CO_2 hydrogenation to methanol. *Catal. Sci. Technol.* **2017**, *7*, 3375-3387. DOI: 10.1039/C7CY01021D.
38. Yang, Y.; Mims, C. A.; Disselkamp, R. S.; Mei, D.; Kwak, J. H.; Szanyi, J.; Peden, C. H. F.; Campbell, C. T. Isotopic Effects in Methanol Synthesis and the Reactivity of Copper Formates on a Cu/SiO_2 Catalyst. *Catal. Lett.* **2008**, *125*, 201-208. DOI: 10.1007/s10562-008-9592-4.
39. Baltes, C.; Vukojevic, S.; Schüth, F. Correlation between synthesis, precursor, and catalyst structure and activity of a large set of $CuO/ZnO/Al_2O_3$ catalysts for methanol synthesis. *J. Catal.* **2008**, *258*, 334-344. DOI: 10.1016/j.jcat.2008.07.004.
40. Jo, Y. R.; Koo, B.; Seo, M. J.; Kim, J. K.; Lee, S.; Kim, K.; Han, J. W.; Jung, W.; Kim, B. J. Growth Kinetics of Individual Co Particles Ex-solved on $SrTi_{0.75}Co_{0.25}O_{3-\delta}$ Polycrystalline Perovskite Thin Films. *J. Am. Chem. Soc.* **2019**, *141*, 6690-6697. DOI: 10.1021/jacs.9b01882.
41. Schumann, J.; Kröhnert, J.; Frei, E.; Schlögl, R.; Trunschke, A. IR-Spectroscopic Study on the Interface of Cu-Based Methanol Synthesis Catalysts: Evidence for the Formation of a ZnO Overlayer. *Top. Catal.* **2017**, *60*, 1735-1743. DOI: 10.1007/s11244-017-0850-9.
42. Pacchioni, G.; Cogliandro, G.; Bagus, P. S. Characterization of oxide surfaces by infrared spectroscopy of adsorbed carbon monoxide: a theoretical investigation of the frequency shift of CO on MgO and NiO. *Surf. Sci.* **1991**, *255*, 344-354. DOI: 10.1016/0039-6028(91)90691-K.
43. Hadjiivanov, K. I.; Vayssilov, G. N. Characterization of oxide surfaces and zeolites by carbon monoxide as an IR probe molecule. *Adv. Catal.* **2002**, *47*, 307-511. DOI: 10.1016/S0360-0564(02)47008-3.
44. Miyata, S. Physico-Chemical Properties of Synthetic Hydrotalcites in Relation to Composition. *Clays Clay Miner.* **1980**, *28*, 50-56. DOI: 10.1346/CCMN.1980.0280107.
45. Gao, P.; Li, F.; Xiao, F.; Zhao, N.; Wei, W.; Zhong, L.; Sun, T. Effect of hydrotalcite-containing precursors on the performance of $Cu/Zn/Al/Zr$ catalysts for CO_2 hydrogenation:

Introduction of Cu^{2+} at different formation stages of precursors. *Catal. Today* **2012**, *194*, 9-15. DOI: 10.1016/j.cattod.2012.06.012.

46. Sanguineti, P. B.; Baltanás, M. A.; Bonivardi, A. L. Copper-gallia interaction in Cu-Ga_2O_3-ZrO_2 catalysts for methanol production from carbon oxide(s) hydrogenation. *Appl. Catal. A-Gen.* **2015**, *504*, 476-481. DOI: 10.1016/j.apcata.2014.11.021.
47. Clarke, D. B.; Suzuki, I.; Bell, A. T. An Infrared Study of the Interactions of CO and CO_2 with Cu/SiO_2. *J. Catal.* **1993**, *142*, 27-36. DOI: 10.1006/jcat.1993.1186.
48. Xu, F.; Mudiyanselage, K.; Baber, A. E.; Soldemo, M.; Weissenrieder, J.; White, M. G.; Stacchiola, D. J. Redox-Mediated Reconstruction of Copper during Carbon Monoxide Oxidation. *J. Phys. Chem. C* **2014**, *118*, 15902-15909. DOI: 10.1021/jp5050496.
49. Dulaurent, O.; Courtois, X.; Perrichon, V.; Bianchi, D. Heats of Adsorption of CO on a Cu/Al_2O_3 Catalyst Using FTIR Spectroscopy at High Temperatures and under Adsorption Equilibrium Conditions. *J. Phys. Chem. B* **2000**, *104*, 6001-6011. DOI: 10.1021/jp9943629.
50. Meng, T.; Ren, N.; Ma, Z. Silicalite-1@Cu-ZSM-5 core-shell catalyst for N_2O decomposition. *J. Mol. Catal. A Chem.* **2015**, *404-405*, 233-239. DOI: 10.1016/j.molcata.2015.05.006.
51. Meng. X.; Yuan, L.; Guo, H.; Hou, B.; Chen, C.; Sun, D.; Wang, J.; Li. D. Carbonylation of methanol to methyl acetate over Cu/TiO_2-SiO_2 catalysts: Influence of copper precursors. *Mol. Catal.* **2018**, *456*, 1-9. DOI: 10.1016/j.mcat.2018.06.022.
52. Hadjiivanov, K.; Knözinger, H. FTIR study of CO and NO adsorption and coadsorption on a Cu/SiO_2 catalyst: Probing the oxidation state of copper. *Phys. Chem. Chem. Phys.* **2001**, *3*, 1132-1137. DOI: 10.1039/B009649K.
53. Toyir, J.; Ramírez de la Piscina, P.; Fierro, J. L. G.; Homs, N. Catalytic performance for CO_2 conversion to methanol of gallium-promoted copper-based catalysts: influence of metallic precursors. *Appl. Catal. B: Environ.* **2001**, *34*, 255-266. DOI: 10.1016/S0926-3373(01)00203-X.
54. Wang, Y.; Zhong, Z.; Liu, T.; Liu, G.; Hong, X. Cu@UiO-66 Derived Cu^+-ZrO_2 Interfacial Sites for Efficient CO_2 Hydrogenation to Methanol. *Acta Phys. - Chim. Sin.* **2021**, *37*, 2007089. DOI: 10.3866/PKU.WHXB202007089.
55. Olah, G. A. Beyond oil and gas: the methanol economy. *Angew. Chem. Int. Ed.* **2005**, *44*, *2636-2639*. DOI: 10.1002/anie.200462121.
56. Porosoff, M. D.; Yan, B.; Chen, J. G. Catalytic reduction of CO_2 by H_2 for synthesis of CO, methanol and hydrocarbons: challenges and opportunities. *Energy Environ. Sci.* **2016**, *9*, 62-73. DOI: 10.1039/C5EE02657A.

57. Zhang, Y.; Zhong, L.; Wang, H.; Gao, P.; Li, X.; Xiao, S.; Ding, G.; Wei, W.; Sun, Y. Catalytic performance of spray-dried Cu/ZnO/Al_2O_3/ZrO_2 catalysts for slurry methanol synthesis from CO_2 hydrogenation. *J. CO_2 Util.* **2016**, *15*, 72-82. DOI: 10.1016/j.jcou.2016.01.005.
58. Schumann, J.; Tarasov, A.; Thomas, N.; Schlögl, R.; Behrens, M. Cu,Zn-based catalysts for methanol synthesis: On the effect of calcination conditions and the part of residual carbonates. *Appl. Catal. A: Gen.* **2016**, *516*, 117-126. DOI: 10.1016/j.apcata.2016.01.037.
59. Tisseraud, C.; Comminges, C.; Belin, T.; Ahouari, H.; Soualah, A.; Pouilloux, Y.; Le Valant, A. The Cu-ZnO synergy in methanol synthesis from CO_2, Part 2: Origin of the methanol and CO selectivities explained by experimental studies and a sphere contact quantification model in randomly packed binary mixtures on Cu-ZnO coprecipitate catalysts. *J. Catal.* **2015**, *330*, 533-544. DOI: 10.1016/j.jcat.2015.04.035.
60. Dasireddy, V. D. B. C.; Likozar, B.; The role of copper oxidation state in Cu/ZnO/Al_2O_3 catalysts in CO_2 hydrogenation and methanol productivity. *Renew. Energy* **2019**, *140*, 452-460. DOI: 10.1016/j.renene.2019.03.073.
61. Chen, Y.; Hong, H.; Cai, J.; Li, Z. Highly Efficient CO_2 to CO Transformation over Cu-Based Catalyst Derived from a CuMgAl-Layered Double Hydroxide (LDH). *Chem. Cat. Chem.* **2021**, *13*, 656-663. DOI: 10.1002/cctc.202001611.
62. Collins, S. E.; Baltanás, M. A.; Bonivardi, A. L. An infrared study of the intermediates of methanol synthesis from carbon dioxide over Pd/β-Ga_2O_3. *J. Catal.* **2004**, *226*, 410-421. DOI: 10.1016/j.jcat.2004.06.012.
63. Solis-Garcia, A.; Fierro-Gonzalez, J. C. Mechanistic Insights into the CO_2 Methanation Catalyzed by Supported Metals: A Review. *J. Nanosci. Nanotechnol.* **2019**, *19*, 3110-3123. DOI: 10.1166/jnn.2019.16606.
64. Calatayud, M.; Collins, S. E.; Baltanás, M. A.; Bonivardi, A. L. Stability of formate species on β-Ga_2O_3. *Phys. Chem. Chem. Phys.* **2009**, *11*, 1397-1405. DOI: 10.1039/B800519B.
65. Borchert, H.; Jürgens, B.; Zielasek, V.; Rupprechter, G.; Giorgio, S.; Henry, C. R.; Bäumer, M. Pd nanoparticles with highly defined structure on MgO as model catalysts: An FTIR study of the interaction with CO, O_2, and H_2 under ambient conditions. *J. Catal.* **2007**, *247*, 145-154. DOI: 10.1016/j.jcat.2007.02.002.
66. Collins, S. E.; Baltanás, M. A.; Bonivardi, A. L. Infrared Spectroscopic Study of the Carbon Dioxide Adsorption on the Surface of Ga_2O_3 Polymorphs. *J. Phys. Chem. B* **2006**, *110*, 5498-5507. DOI: 10.1021/jp055594c.
67. Zhao, K.; Wang, L.; Calizzi, M.; Moioli, E.; Züttel, A. In Situ Control of the Adsorption Species in CO_2 Hydrogenation: Determination of Intermediates and Byproducts. *J. Phys. Chem. C* **2018**, *122*, 20888-20893. DOI: 10.1021/acs.jpcc.8b06508.

68. Van Rensburg, W. J.; Petersen, M. A.; Datt, M. S.; Van der Berg, J. A.; Van Helden, P. On the Kinetic Interpretation of DFT-Derived Energy Profiles: Cu-Catalyzed Methanol Synthesis. *Catal. Lett.* **2015**, *145*, 559-568. DOI: 10.1007/s10562-014-1407-1.
69. Clarke, D. B.; Bell, A. T. An Infrared Study of Methanol Synthesis from CO_2 on Clean and Potassium-Promoted Cu/SiO_2. *J. Catal.* **1995**, *154*, 314-328. DOI: 10.1006/jcat.1995.1173.
70. Bando, K. K.; Sayama, K.; Kusama, H.; Okabe, K.; Arakawa, H. In-situ FT-IR study on CO_2 hydrogenation over Cu catalysts supported on SiO_2, Al_2O_3, and TiO_2. *Appl. Catal. A: Gen.* **1997**, *165*, 391-409. DOI: 10.1016/S0926-860X(97)00221-4.
71. Busca, G.; Lorenzelli, V. Infrared spectroscopic identification of species arising from reactive adsorption of carbon dioxide on metal oxide surfaces. *Mater. Chem.* **1982**, *7*, 89-126. DOI: 10.1016/0390-6035(82)90059-1.
72. Yang, Y.; Mims, C. A.; Disselkamp, R. S.; Kwak, J. H.; Peden, C. H. F.; Campbell, C. T. (Non)formation of Methanol by Direct Hydrogenation of Formate on Copper Catalysts. *J. Phys. Chem. C* **2010**, *114*, 17205-17211. DOI: 10.1021/jp104068k.

TOC GRAPHIC